A Fiber-Optic Temperature Sensor Based on Dual Fluorescence by Using FIR Method

Du Xinchao[1,2] Zhou Libin[3] He Zhengquan[1] Liu Feng[1] Lin Xiao[1,2] Hu Baowen[1]
Guo Xiaoyi[1] Luo Baoke[1] Ren Liyong[1] Li Yulin[1]

[1]*Xi'an Institute of Optics and Precision Mechanics, Chinese Academy of Sciences, Xi'an, Shaanxi* 710119, *China*
[2]*University of Chinese Academy of Sciences, Beijing* 100049, *China*
[3]*Department of Physics, Northwest University, Xi'an, Shaanxi* 710069, *China*

Abstract A fiber-optic temperature sensor based on fluorescence intensity ratiometric (FIR) method is proposed and investigated experimentally. Plastic optical fibers are employed for transmitting the excitation light and collecting the Rhodamine B (RHB) and Rhodamine110 (RH110) fluorescence signals. Given that the fluorescence intensity of RHB is temperature-dependent while that of RH110 is temperature-independent, the temperature can be measured by calculating the fluorescence intensity ratio of these two dyes. To achieve a desired performance, the optimal integration ranges of fluorescence intensities of the two dyes are identified via considerable experimental tests. Indeed, a precise measurement is achieved in experiments. The feasible range of temperatures is from 25 ℃ to 60 ℃; a minimum rms temperature error of 0.38 ℃ and a sensitivity of 0.0134 /℃ are achieved. Further, the proposed sensor is proved to be insensitive to fiber bending for bend radii exceeding 9 mm. Thus, the sensor can be used for in situ temperature monitoring.

Key words fiber optics; fluorescence intensity ratiometric; spectral interval; temperature sensor; plastic optical fiber

OCIS codes 060.2300; 060.2370; 120.6780; 130.6010

一种基于双荧光比值法的光纤温度传感器

杜新超[1,2] 周利斌[3] 贺正权[1] 刘 丰[1] 林 霄[1,2] 胡宝文[1] 郭小艺[1] 罗宝科[1] 任立勇[1] 李育林[1]

[1]中国科学院西安光学精密机械研究所, 陕西 西安 710119
[2]中国科学院大学, 北京 100049
[3]西北大学物理学院, 陕西 西安 710069

摘要 提出了一种基于荧光强度比值法的光纤温度传感器并通过实验来具体探究其性能。实验中采用塑料光纤来传导激励光,以及接收罗丹明B和罗丹明110两种荧光物质发出的荧光。由于罗丹明B对温度敏感而罗丹明110对温度不敏感,因此可通过计算两种物质的荧光强度比来标定温度。为了得到理想的测温性能,进行了大量实验以确定出可用于比值法的最佳荧光光谱范围。该传感器在25~60 ℃的范围内能稳定工作,可获得0.38 ℃的最小均方误差及0.0134 /℃的灵敏度。此外,通过实验证明该传感器对曲率半径大于9 mm的光纤弯曲不敏感;在现场温度测量方面有较大的应用潜力。

关键词 光纤光学; 荧光强度比率; 谱间隔; 温度传感器; 塑料光纤

中图分类号 O439 **文献标识码** A

doi: 10.3788/CJL201542.0805002

收稿日期: 2015-01-25; **收到修改稿日期**: 2015-03-23

基金项目: 国家自然科学基金(61275086,61275149)

作者简介: 杜新超(1989—),男,硕士研究生,主要从事光纤传感器方面的研究。E-mail: duxinchao@opt.ac.cn

导师简介: 贺正权(1965—),男,硕士,研究员,主要从事生物医学成像、三维物体重建等方面的研究。

E-mail: zhqhe@opt.ac.cn(通信联系人)

1 Introdution

Fiber-optic temperature sensors have been studied for over four decades and are of particular interest owing to their advantages over their electric counterparts; these advantages include compact size, high safety, and immunity to electromagnetic interferences (EMI). The temperature sensors based on silica optical fibers can be implemented in a number of ways, such as fiber grating, stimulated Brillouin scattering (SBS), and Mach-Zehnder interferometer[1-4]. However, silica optical fibers can be easily broken, and are not as low-cost and flexible as plastic optical fibers (POFs). Regarding the POF temperature sensors, precise measurements are achieved by detecting the spectral shift[5-7], where a complex system is usually applied. As is well known, the POF sensors are always established based on intensity modulation technique with simple configurations[8-9]. Hence, in real applications, an intensity-based POF temperature sensor with simple structure is expected to achieve high measurement precision, and the fluorescence method is a promising approach for achieving this goal.

In general, there are three schemes that can be employed for measuring the temperature by using the fluorescence method: 1) the steady state fluorescence intensity method; 2) the fluorescence lifetime method; 3) the fluorescence intensity ratiometric (FIR) method. The steady state fluorescence intensity method is the most direct way. However, the measurement results may be influenced by some artefacts owing to the non-temperature related changes in the fluorescence intensity[10-11]. High precision can be achieved by using the lifetime method; however, a pulsed light source and fast response electronics are required for this, making the setup expensive[12]. The FIR method has been studied extensively owing to its ability to mitigate or eliminate external perturbations, such as the power fluctuations of the excitation light source, variation in transmission loss in the optical pass, and the photo-bleaching effect of dyes[13-17]. In this scheme, two types of fluorophores, which are temperature-dependent and temperature-independent respectively, are utilized for temperature calibration. Ideally, it can be assumed that photo-bleaching affects the fluorescence bands of the two fluorophores in the same way[18]. As a result, the intensity ratio of the two corresponding fluorescence bands only depends on the temperature. Hence, the FIR method is a technique providing a self-referenced measurement, which is beneficial for an accurate and reliable performance of the sensor system.

A fiber-optic temperature sensor based on the FIR method is demonstrated. Two types of low-cost and commercially available fluorescent dyes, Rhodamine B (RHB) and Rhodamine110 (RH110), which serve as the temperature indicator and reference indicator respectively, are encapsulated in a stainless steel tube for forming a sensor head. Because the RHB fluorophore is sensitive to the variation of temperature while the RH110 fluorophore is temperature-insensitive, the FIR method can be used for measuring the temperature. Via considerable experimental examinations, the optimal spectral ranges of the two dyes′ fluorescence used to determine the fluorescence intensity are obtained, which is significant for the sensor′s performance. In our scheme, POFs act as a medium for transmitting the excitation light and fluorescence. The corresponding experiment was performed, and the sensor proved to be feasible at temperatures ranging from 25 ℃ to 60 ℃, as demonstrated by the correlated results. Moreover, we also analyzed in detail the effects of fiber bending on the temperature response.

2 Sensor system and operating principle

2.1 The configuration of the whole sensor system

The fabrication of the sensing head is described in detail. The RHB (fluorescence grade, Sigma-Aldrich) solution with concentration of 1 g/L and RH110 (≥99.0% laser grade, Sigma-Aldrich) solution with concentration of 0.5 g/L were prepared in advance, with deionized water as a solvent. The RHB and RH110 solutions were mixed with a volume ratio of 2:3 to form the sensing liquid. After that, 0.3 mL of the sensing liquid was poured into a stainless steel tube. Two identical polymer optical fibers (Super Eska SK-40, Mitsubishi Rayon Co.) were glued together by using two-part epoxy resin, and then dipped into the liquid, as shown in Fig.1. One of the fibers served as the

illumination fiber for transmitting the excitation light, and the other one acted as the detection fiber for collecting the fluorescence signals. Note that the end-faces of the POFs were polished delicately. The POFs, the sensing liquid and the tube were integrated together permanently to form the sensing head. To shorten the response time, it is better to fabricate small-sized sensing heads allowing almost immediate temperature stabilization.

The configuration of the proposed temperature sensor system is shown in Fig.1. The system consists of a sensing head, a tungsten halogen lamp (AvaLight-HAL), a heater with a temperature feedback controller, and a fiber optic spectrometer (AverSpec-2048, Netherlands). The beam emitted from the tungsten halogen lamp is transmitted through a band-pass filter and only the light with wavelengths in the 470~500 nm range is selected as the excitation light. Then, this excitation light is directly injected into the illumination fiber for exciting the fluorophore. The fluorescence irradiated from the fluorophore is captured by the detection fiber; it further propagates back to the spectrometer. The temperature controller is employed for monitoring the temperature of a water bath by using a thermistor as well as for regulating the heater. When the temperature of the water bath is adjusting, the corresponding fluorescence spectrum can be logged by using the spectrometer.

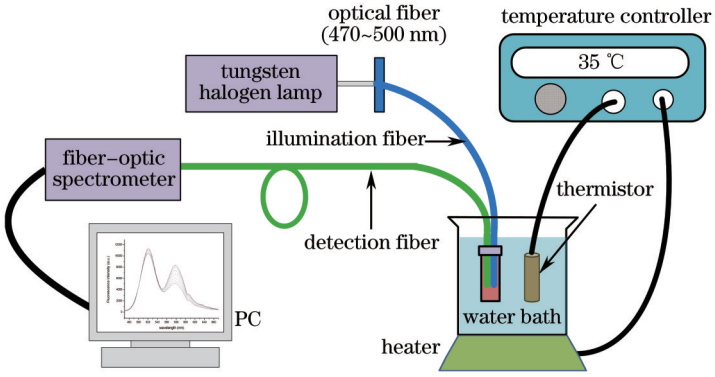

Fig.1 Setup of temperature measurement with FIR method

2.2 The property of the fluorescence dyes and FIR method

The RHB and RH110 fluorophores are ideal candidates for fluorescence intensity ratio measurements[19-20]. The RHB is one of the most widely used temperature sensing indicators. The thermo-optical property of the RHB depends on a number of factors, such as the solvent, concentration, pH value, temperature, and the supporting material if it is immobilized[11]. In our experiment, the RHB concentration was the most important factor that affected the temperature measurements. The absorption spectrum of RHB covers the wavelengths from 470 nm to 600 nm. On the other hand, the absorption spectrum of RH110 covers the wavelengths from 470 nm to 500 nm. The two dyes are water-soluble[20]. Considering that the absorption spectra of the two dyes overlap in the 470~500 nm range, in our system only the blue light source which is obtained by using the tungsten halogen lamp followed by a filter, was employed for pumping the fluorophore.

The relationship between the fluorescence intensity I, and the dye′s concentration C, is[20]:

$$I = I_0 \alpha \phi \varepsilon L C , \tag{1}$$

where ϕ is the quantum efficiency of the fluorophore, ε is the molar absorptivity, α is the collection efficiency, I_0 is the intensity of incident irradiation, and L is the absorption path length.

The intensity ratio of the emission fluorescence of the two dyes, which can be used to measure the temperature, is defined as follows

$$\frac{I_{e\mathrm{RH110}}}{I_{e\mathrm{RHB}}} = \frac{\varepsilon_{\mathrm{RH110}} \alpha_{\mathrm{RH110}} \phi_{\mathrm{RH110}} C_{\mathrm{RH110}}}{\varepsilon_{\mathrm{RHB}} \alpha_{\mathrm{RHB}} \phi_{\mathrm{RHB}} C_{\mathrm{RHB}}} , \tag{2}$$

Although the tungsten halogen lamp with a band-pass filter, instead of a laser, is indeed used as the excitation light source, we can still conclude that the ratio is independent of I_0 and L as is shown by Eq.(2). Meanwhile, ε and α

are considered to be constant over the tested range of temperatures. As long as the concentration is fixed, the intensity ratio only depends on the quantum efficiencies, ϕ_{RHB} and ϕ_{RH110}, which are temperature-sensitive and temperature-insensitive, respectively.

In the experiment, the measured fluorescence intensities represent the intensities integrated over certain spectral intervals, namely, $I_{\mathrm{RH110}}=\int_{\lambda_1}^{\lambda_2} I_{\mathrm{eRH110}}\mathrm{d}\lambda$ and $I_{\mathrm{RHB}}=\int_{\lambda_2}^{\lambda_3} I_{\mathrm{eRHB}}\mathrm{d}\lambda$, where λ_1, λ_2, λ_3 and λ_4 are the endpoints of the selected spectral intervals. Thus, the I_{RH110} to I_{RHB} ratio would vary with temperature and can be used for temperature calibration.

3　Results and discussion

Experimental investigations were conducted to study the performance of the proposed fiber-optic sensor. During the experiment, a water bath was used to heat the sensing head from room temperature of 25 ℃ to 60 ℃, in steps of 1 ℃. Note that it takes about 1 minute for the heating system to reach the preset temperature and 3 minutes more for temperature stabilization. A thermistor with 0.1 °C resolution was used for temperature calibration.

The fluorescence spectra detected by using our sensor system at different temperatures ranging from 25 ℃ to 60 ℃ are shown in Fig.2. The RH110 emission peak is at ~520 nm, while that of RHB is at ~580 nm. Hence, the two peaks are about 60 nm apart and the interference between them is weak. Meanwhile, it can also be seen that the peaks are isolated from the excitation wavelengths. When the temperature rises, the RHB emission peak′s intensity decreases significantly. As for the RH110 fluorescence spectrum, it is assumed to be temperature-insensitive. However, it is observed that the RH110 emission peak′s intensity fluctuates slightly, which may be caused by the photo-bleaching of RH110, the fluctuations of the excitation light source, and the overlap of the RH110 and RHB spectra. Although this fluctuation exists, it is demonstrated to have little influence on the sensor′s performance[19-20]. In addition, it is noteworthy that no shifts occurred in the emission spectra when the temperature changed.

Actually, above 60 ℃, the RHB fluorescence intensity is much lower; as the temperature continues to rise, the reduction in the fluorescence intensity becomes insignificant. In addition, the POF should not be exposed to a high temperature for the sake of its lifetime. Below 25 ℃, the ratio of RH110 to RHB intensities is not linear. Thus, the feasible range of temperatures is from 25 ℃ to 60 ℃.

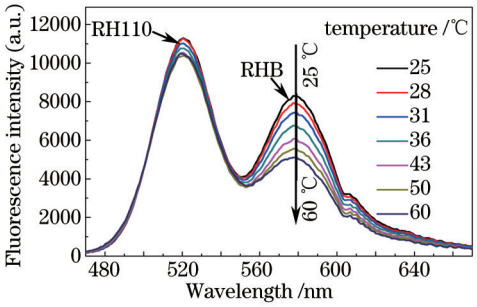

Fig.2　Emission spectra of the mixture of RHB and RH110, at different temperatures. The spectra were recorded while heating the sensing head from 25 ℃ to 60 ℃

Considering that the measured fluorescence intensities, I_{RH110} and I_{RHB}, represent integrations over certain spectral intervals, the ratio of these two intensities is determined by the spectral intervals. Hence, to achieve an excellent performance of the sensor, it is critical to identify the optimal spectral intervals of the RH110 and RHB. Firstly, three spectral intervals with different widths, 565~595 nm, 570~590 nm, 575~585 nm, all centered at 580 nm, are selected as the integration intervals of I_{RHB}, respectively. As for RH110, based on the discussion in the previous paragraph, the 495~545 nm wavelengths range is preferably employed for representing the fluorescence spectrum of RH110. For identifying the optimal spectral interval of RH110, the 495~545 nm wavelengths range is divided into four groups of spectral intervals with four different widths respectively, and each of these spectral intervals is selected for examining

the sensor′s performance. The four groups of spectral intervals with the widths of 32, 26, 20, and 14 nm are illustrated in Table 1. For each group, the increment between two adjacent spectral intervals is 3 nm. As the candidates of spectral intervals for RHB and RH110 are determined, all the corresponding integrated intensities, I_{RHB}s and I_{RH110}s, are obtained.

Table 1　Candidate spectral intervals (in nm) for RH110

Width /nm	Sequence number of spectra interval											
	1	2	3	...	6	7	8	9	10	11	12	13
32	495~527	498~530	501~533	…	510~542	513~545						
26	495~521	498~524	501~527	…	510~536	513~539	516~542	519~545				
20	495~515	498~518	501~521	…	510~530	513~533	516~536	519~539	522~542	525~545		
14	495~509	498~512	501~515	…	510~524	513~527	516~530	519~533	522~534	525~539	528~542	531~545

Now the sensor′s performance with the measured spectra is analyzed, when each of the spectral intervals of RHB and RH110 (shown in Table 1) is concerned. Initially, the 565~595 nm interval is set as the interval of I_{RHB}. Then, each of the intervals in Table 1 is selected as the interval of I_{RH110} respectively. Thus, there are forty combinations of intervals for FIR implementation. For each of these different combinations, the ratios of I_{RH110} and I_{RHB} in the 25~60 ℃ range can be obtained, corresponding to the temperature calibration curve in our experiment. Here, I_{RH110} and I_{RHB} are normalized relative to their values at 25 ℃[19-20]. Likewise, when the 570~590 nm and 575~585 nm intervals are also set as the I_{RHB} intervals, we obtain eighty combinations that can be employed for temperature calibration.

After examining 120 combinations of intervals by using the FIR method, it is found that the I_{RH110} to I_{RHB} ratio scales almost linearly with temperature. Linear regression can be used to express this dependence as $r=kT+b$, where k and b denote the slope and the intercept, respectively; r refers to the measured ratio, and T is the temperature in degrees Celsius. The measurement errors of the proposed fiber-optic temperature sensor are also obtained by using the linear fitting equation. It is concluded that 575~585 nm for RHB and 531~545 nm for RH110 are the optimal spectral intervals for temperature measurement, with the maximum adjusted R-squared value of 0.999 and minimum rms temperature error of 0.38 ℃.

To demonstrate how the RH110 intervals affect the sensor′s performance, the slopes and the rms temperature errors obtained with different intervals for RH110 and with 575~585 nm interval for RHB, are plotted in Fig.3. As can be seen, the rms temperature errors in Figs.3(a)~(d) monotonically decrease as the spectral interval shifts toward longer

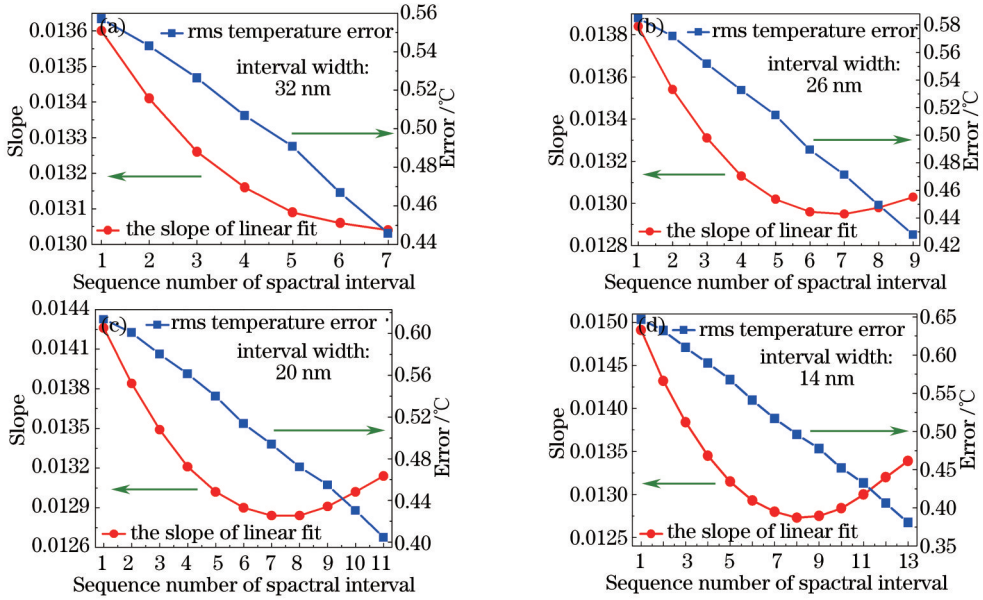

Fig.3　When the 575~585 nm interval is set for RHB, different spectral intervals of RH110 are selected for temperature detection by using the FIR method, and the corresponding slopes of the linear fitting curves as well as the measurement errors are given

wavelengths. Note that the rms temperature error decreases from 0.45 ℃ to 0.38 ℃ as the spectral width diminishes. On the other hand, the slope in Fig.3(a) shows a monotonous decrease as the interval approaches 545 nm; but with the interval width diminishing, as illustrated in Figs.3(b)~(d), the slope initially decreases when the interval is 495~530 nm and then increases above 0.130 for the 530~545 nm interval.

The I_{RHB} and I_{RH110} at various temperatures by using the optimal spectral interval are shown in Fig.4(a). For comparison, the other two curves for I_{RH110}s, corresponding to the spectral intervals of 495~527 nm and 507~527 nm, are also shown in the same figure. It can be seen that I_{RHB} decreases with increasing temperature while I_{RH110} is almost constant over the whole range of temperatures. Fig.4(b) illustrates three ratiometric results calculated for three spectral intervals of RH110. It is obvious that the rms temperature error decreases as the selected interval of RH110 approaches longer wavelengths, namely 531~545 nm. The thermal response of the ratios in Fig.4(b), by using linear regression, can be expressed as:

$$\begin{cases} r_1 = 0.0134T + 0.6775 \\ r_2 = 0.0130T + 0.6868 \\ r_3 = 0.0134T + 0.6731 \end{cases}, \tag{3}$$

where r_1, r_2, and r_3 refer to the ratios obtained by using the three spectral intervals of RH110 in Fig.4(b), at different temperatures. The adjusted R− squared values are 0.997, 0.997 and 0.999, demonstrating a good linearity of regression. The rms deviations of the data are 0.007281, 0.007029, and 0.005154 for the spectral intervals of 495~527 nm, 507~527 nm, and 531~545 nm, resulting in the rms temperature errors of 0.56 ℃, 0.53 ℃, 0.38 ℃, over the whole range of temperatures, respectively.

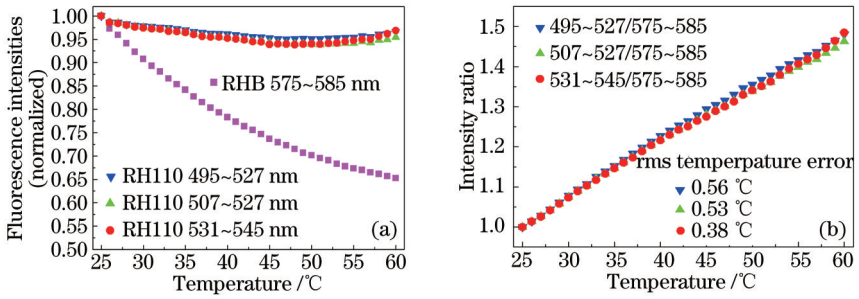

Fig.4 (a) Fluorescence intensities of RHB and RH110 are acquired by integrating the intensity (a.u.) over the certain intervals. (b) ratios of I_{RHB} and I_{RH110} are obtained and the corresponding rms temperature errors are given

4 Fiber bending effects

Fiber bending is inevitable in most practical applications. The output intensity from a bent fiber would change depending on the radius of curvature. As is reported previously[10-11], fiber−optic temperature sensors based on the steady state fluorescence intensity method are not capable of eliminating the intensity fluctuations in optical pass, such as those caused by fiber bending. Thus, these intensity changes during measurement would be incorrectly interpreted as temperature variations.

To evaluate the bending−resistance ability of the proposed sensor, correlated experiments are conducted to test the effects of different bend radii on the sensor′s performance. The principal measured quantity in our experiment is the I_{RH110} to I_{RHB} ratio. Initially, an experiment without fiber bending was conducted for obtaining the intensity ratios at various temperatures, and the measured results are plotted in Fig.5 (a). Then, three glass cylinders, with bend radii of 20.0, 13.0 and 9.0 mm, were used for bending the POF for a full turn to examine the influence of bending, respectively. While the POF was bent with one of the cylinders, the corresponding measured intensity ratios at different temperatures were acquired and are shown in Figs.5(b)~(d). Note that the overall fiber length and launching conditions were constant throughout the different experiments.

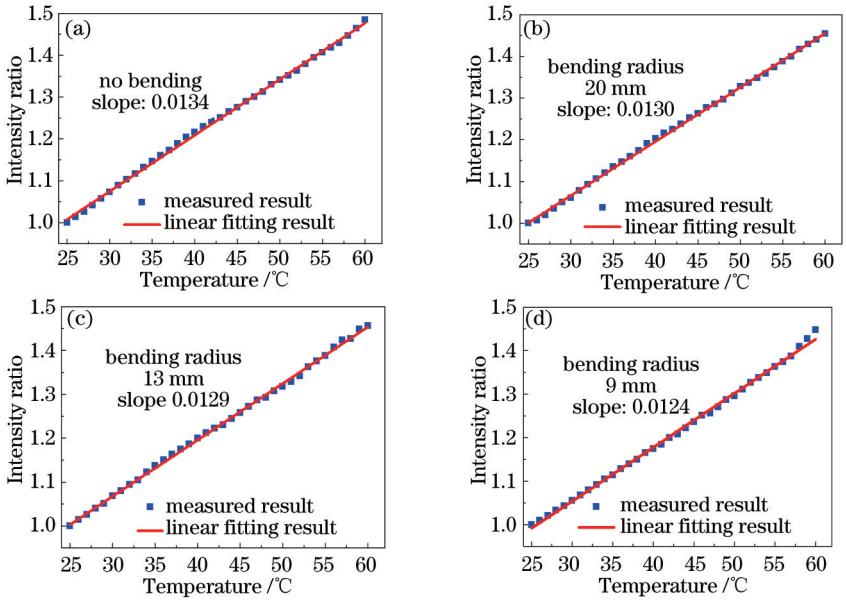

Fig.5 Linear fitting results of the ratio responses versus temperature with different bend radii are compared

In Fig.5 we show the linear fitting results for the measured ratios, for different bend radii. When the bend radii were infinite (no bend), 20, 13 and 9 mm, the adjusted R-square values were 0.999, 0.999, 0.999, 0.998, showing good linear regression. The corresponding slopes (sensitivity) were 0.0134 (±0.005154)/ ℃, 0.0130 (±0.004122) /℃, 0.0129 (±0.004515)/ ℃ and 0.0124 (±0.005963)/ ℃, and the corresponding temperature errors over the whole range of temperatures were 0.38 ℃, 0.32 ℃, 0.35 ℃, and 0.48 ℃, respectively. It is conspicuous that the fitted slope decreased with decreasing bend radii. Actually, compared with the non-bent POF, the output fluorescence intensity from a bent POF would decrease with decreasing radius owing to the bending loss[21]. To evaluate these intensity reductions induced by the bending with bend radii of 20, 13, and 9 mm, the I_{RH110} and I_{RHB} obtained with the spectrum of 25 ℃ (as the black curve illustrated in Fig.2) for each measurement are used for analysis. The attenuation coefficients of I_{RH110} and I_{RHB} in decibels relative to the non-bent POF are shown in Table 2. It is noted that when the bend radius is 9 mm, the slope decreases significantly. This is owing to the losses caused by a small radius bend, which results in a sharp reduction of the fluorescence intensity. The attenuation coefficients of I_{RH110} and I_{RHB} in decibels relative to the non-bent POF are −2.47 and −1.76, respectively. Moreover, it is observed that the attenuation coefficient of I_{RH110} differs from that of I_{RHB}. This wavelength dependence of the received fluorescence intensity can be attributed to tunneling rays and to the core refractive index with wavelength[22].

Table 2 Attenuation coefficients of I_{RH110} and I_{RHB} in decibels relative to the unbent POF

	Attenuation coefficients	
Bend radius /mm	I_{RH110}	I_{RHB}
20	−0.06	−0.15
13	−1.47	−0.77
9	−2.47	−1.76

Therefore, it can be concluded that for the bend radii exceeding 13 mm, the effect of bend loss on the measured slope is negligible to some extent. Fortunately, bend radii below 13 mm are quite infrequent in practical fiber-optic systems and installations. The results demonstrate that our approach is partially capable of eliminating the transmission loss caused by fiber bending.

5 Conclusion

A robust fiber-optic temperature sensor with a simple structure for in situ measurement is demonstrated. Based on the FIR method, it is observed that the ratio of the fluorescence intensities of RH110 and RHB is linear in

temperature for temperatures ranging from 25 ℃ to 60 ℃. By studying the effects of spectral intervals of I_{RH110} and I_{RHB} on the sensor′s performance, it can be concluded that the bands of 531~545 nm and 575~585 nm are the optimal integration ranges for I_{RH110} and I_{RHB}, respectively. In fact, we have fabricated three sensing liquids, each having different concentrations of the dyes, and the optimal integration ranges for the fluorescence intensities of the two dyes exhibited no shifts. In the experiment, a sensitivity of 0.0134/℃ and a minimum rms temperature error of 0.38 ℃ were obtained. Further, experimental investigations on the influence of fiber bend on the measurement were also conducted, verifying the robustness of our sensor with respect to fiber bending, for bend radii exceeding 13 mm. In addition, although a compatible fiber-optic spectrometer is utilized for monitoring the fluorescence signal in this work, it can be replaced by a pair of photo-diodes with appropriate band pass filters. Thus, a low-cost fiber-optic temperature sensor can be fabricated in future, and potentially used for temperature monitoring of fermentation and concrete hydration processes. The performance of the sensing device may be improved by choosing more superior fluorescent dyes.

References

1 Lang Yue, Tong Shoufeng. Design of demodulation system of fiber Bragg grating temperature sensor based on FPGA[J]. Laser & Optoelectronics Progress, 2013, 50(9): 090601.
郎　月, 佟首峰. 基于FPGA的FBG温度传感器解调系统设计[J]. 激光与光电子学进展, 2013, 50(9): 090601.

2 Lü Weiwei, Xu Feng, Yu Benli. All-fiber Mach-Zehnder temperature sensor based on inter-modal interference[J]. Laser & Optoelectronics Progress, 2014, 51(5): 050605.
吕卫卫, 徐　峰, 俞本立. 基于模间干涉原理的全光纤马赫-曾德尔温度传感器[J]. 激光与光电子学进展, 2014, 51(5): 050605.

3 Huang Wenfa, Wang Xiaochao, Wang Jiangfeng, *et al*.. Temperature characteristic of stimulated brillouin scattering in single-mode fiber[J]. Chinese J Lasers, 2013, 40(4): 0405001.
黄文发, 汪小超, 王江峰, 等. 单模光纤中受激布里渊散射的温度特性[J]. 中国激光, 2013, 40(4): 0405001.

4 Pan Hongliang, Dong Huijuan, Zhang Guangyu, *et al*.. Research on fiber grating pressure/temperature monitoring device of distinguish range and double sensitivity[J]. Chinese J Lasers, 2013, 40(2): 0205005.
潘洪亮, 董惠娟, 张广玉, 等. 分程式双灵敏度光纤光栅压力/温度监测装置的研制[J]. 中国激光, 2013, 40(2): 0205005.

5 A Minardo, R Bernini, L Zeni. Distributed temperature sensing in polymer optical fiber by BOFDA[J]. Photonics Technology Letters, IEEE, 2014, 26(4): 387-390.

6 Y Mizuno, K Nakamura. Potential of Brillouin scattering in polymer optical fiber for strain-insensitive high-accuracy temperature sensing[J]. Opt Lett, 2010, 35(23): 3985-3987.

7 Y Luo, W Wu, T Wang, *et al*.. Analysis of multimode BDK doped POF gratings for temperature sensing[J]. Opt Commun, 2012, 285 (21): 4353-4358.

8 H A Rahman, S W Harun, N Saidin, *et al*.. Fiber optic displacement sensor for temperature measurement[J]. Sensors Journal, IEEE, 2012, 12(5): 1361-1364.

9 X Lin, L Ren, Y Xu, *et al*.. Low-cost multipoint liquid-level sensor with plastic optical fiber[J]. Photonics Technology Letters, IEEE, 2014, 26(16): 1613-1616.

10 S Tao, A Jayaprakash. A fiber optic temperature sensor with an epoxy-glue membrane as a temperature indicator[J]. Sensors and Actuators B: Chemical, 2006, 119(2): 615-620.

11 H D Duong, J I Rhee. Exploitation of thermo-effect of rhodamine B entrapped in sol-gel matrix and silica gel for temperature detection[J]. Sensors and Actuators B: Chemical, 2007, 124(1): 18-23.

12 Z Zhang, K T V Grattan, A W Palmer. Fiber-optic high-temperature sensor based on the fluorescence lifetime of alexandrite[J]. Review of scientific Instruments, 1992, 63(8): 3869-3873.

13 H Aizawa, T Katsumata, S Komuro, *et al*.. Fluorescence thermometer based on the photoluminescence intensity ratio in Tb doped phosphor materials[J]. Sensors and Actuators A: Physical, 2006, 126(1): 78-82.

14 J Castrellon-Uribe. Experimental results of the performance of a laser fiber as a remote sensor of temperature[J]. Optics and Lasers in Engineering, 2005, 43(6): 633-644.

15 D Li, Y Wang, X Zhang, *et al*.. Optical temperature sensor through infrared excited blue upconversion emission in Tm^{3+}/Yb^{3+} codoped Y_2O_3[J]. Opt Commun, 2012, 285(7): 1925-1928.

16 J Castrellon, G Paez, M Strojnik. Radiometric analysis of a fiber optic temperature sensor[J]. Opt Eng, 2002, 41(6): 1255-1261.

17 L Liu, Y Wang, X Zhang, *et al*.. Optical thermometry through green and red upconversion emissions in $Er^{3+}/Yb^{3+}/Li^{+}$: ZrO_2 nanocrystals[J]. Opt Commun, 2011, 284(7): 1876-1879.

18 H T Lam, Y Kostov, L Tolosa, *et al*.. A high-resolution non-contact fluorescence-based temperature sensor for neonatal care[J]. Measurement Science and Technology, 2012, 23(3): 035104.

19 P Chamarthy, S V Garimella, S T Wereley. Measurement of the temperature non-uniformity in a microchannel heat sink using microscale laser-induced fluorescence[J]. International Journal of Heat and Mass Transfer, 2010, 53(15): 3275-3283.

20 J Sakakibara, R J Adrian. Whole field measurement of temperature in water using two-color laser induced fluorescence[J]. Experiments in Fluids, 1999, 26(1-2): 7-15.

21 X Lin, L Ren, J Liang. Nondestructive scheme for measuring the attenuation coefficient of polymer optical fiber[J]. Opt Lett, 2013, 38(4): 528-530.

22 G Durana, J Zubia, J Arrue, *et al*.. Dependence of bending losses on cladding thickness in plastic optical fibers[J]. Appl Opt, 2003, 42(6): 997-1002.

栏目编辑：苏　岑